LASER
& PHOTONICS
REVIEWS

Laser Photonics Rev. **9,** No. 1, 91–97 (2015) / **DOI** 10.1002/lpor.201400132

Abstract A novel scheme to multiply the repetition rate of a monolithic self-mode-locked laser for generating sub-terahertz pulse sources is successfully demonstrated. A coated Yb:KGW crystal is designed to achieve a self-mode-locked operation at a repetition rate of 24 GHz with an average output power exceeding 1.0 W at a pump power of 4.8 W. A partially reflective mirror is utilized to combine with the output surface of the gain medium to constitute an external Fabry-Perot cavity. It is theoretically and experimentally verified that adjusting the external cavity length to satisfy the commensurate condition can lead to the frequency spacing to be various order harmonics of the mode spacing of the monolithic cavity. The maximum pulse repetition rate of the laser output can be up to 216 GHz and the pulse duration is as short as 330 fs. More importantly, the overall characteristics of the first-order temporal autocorrelation traces obtained by sequentially scanning the external cavity.length display an intriguing phenomenon of temporally fractional revivals, similar to the feature of spatial Talbot revivals.

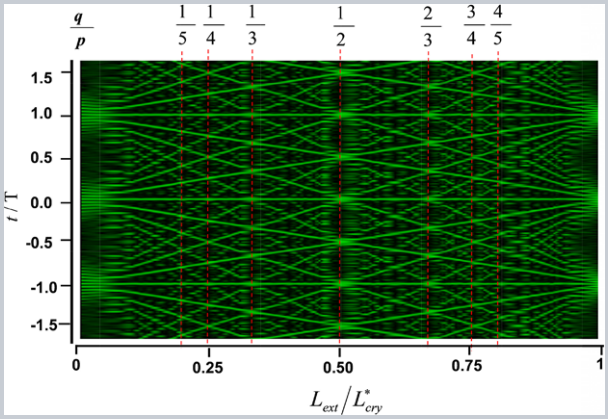

ORIGINAL PAPER

Generation of sub-terahertz repetition rates from a monolithic self-mode-locked laser coupled with an external Fabry-Perot cavity

Y. F. Chen[1,2,*], M. T. Chang[1], W. Z. Zhuang[1], K. W. Su[1], K. F. Huang[1], and H. C. Liang[3]

1. Introduction

Techniques for developing high-repetition-rate optical pulses are particularly attractive for applications such as optical frequency comb spectroscopy [1], high capacity optical networks [2], spectroscopy of metallic nanoparticles [3], and arbitrary waveform generation [4]. The promising approaches include the mode locking in laser resonators [5–8] and the four-wave mixing in micro-cavities [9–12]. It is an interesting phenomenon to achieve the self-mode-locking without using active elements or saturable absorbers. The Kerr-lens mode-locked Ti-sapphire laser is the first demonstration of self-mode-locking. Noticeably, the self-mode-locking has recently been realized in various diode-pumped crystal lasers comprising Yb:$KY(WO_4)_2$ [13], Yb:$KGd(WO_4)_2$ [14], Yb:YVO_4 [15], Yb:Y_2O_3 [16], Yb:YAG [17], Nd:YVO_4 [18,19], and Nd:$GdVO_4$ [20] crystals. Thanks to the self-mode-locked operation, the repetition rate can be up to several tens of GHz with a monolithic resonator [14]. Nowadays, repetition-rate scale up of periodic pulse sources is significantly important for the increasing demand in ultrahigh-speed optical communications. One of the most appealing methods for scaling up the pulse rate is to multiply the repetition rate of a lower rate source [21–28]. Therefore, discovering a technique to multiply the repetition rate of a compact self-mode-locked laser will be greatly prospective for generating ultrahigh-repetition-rate sources.

In this work we successfully demonstrate a novel scheme to multiply the repetition rate of a monolithic self-mode-locked laser for generating sub-terahertz pulse sources. Referring to Fig. 1, we design a coated Yb:KGW crystal to achieve the monolithic self-mode-locked operation at a repetition rate of $f_{ML} = 24$ GHz with an average output power exceeding 1.0 W at a pump power of 4.8 W. We then utilize a partially reflective mirror to be closely behind the monolithic laser to form an external Fabry-Perot (FP) cavity. We numerically verify that adjusting the external cavity length L_{ext} to satisfy the commensurate condition of $L_{ext}/L^*_{cry} = q/p$ can lead to the frequency spacing to be the pth order harmonics of the mode spacing of the monolithic cavity, i.e. $p \times f_{ML}$, where L^*_{cry} and L_{ext} are the optical lengths of the monolithic crystal and the external FP cavity, respectively. We further experimentally confirm that the laser output with pulse rates up to 216 GHz can be generated by scanning the external FP cavity length and the pulse rates are integer multiples of the repetition rate f_{ML}. Moreover, we also find that the first-order

[1] Department of Electrophysics, National Chiao Tung University, 1001 Ta-Hsueh Rd., Hsinchu 30010, Taiwan
[2] Department of Electronics Engineering, National Chiao Tung University, 1001 Ta-Hsueh Rd., Hsinchu 30010, Taiwan
[3] Institute of Optoelectronic Science, National Taiwan Ocean University, Keelung 20224, Taiwan
*Corresponding author: e-mail: yfchen@cc.nctu.edu.tw

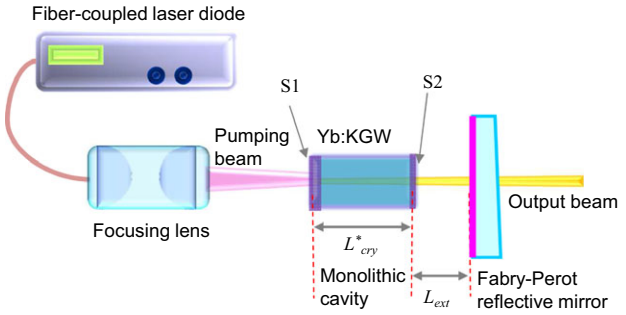

Figure 1 Schematic diagram of the system setup including a monolithic self-mode-locked laser and an external FP feedback cavity. S1: the surface that faces the pump source and that acts as the resonator high-reflectivity mirror and S2: the opposite side.

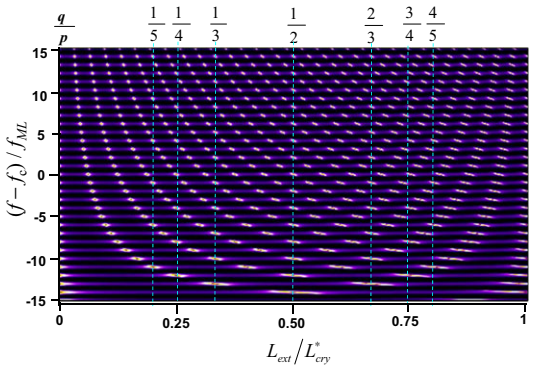

Figure 2 Numerical results for the frequency spectrum as a function of the ratio L_{ext}/L^*_{cry} in the range of 0.0−1.0.

temporal autocorrelation traces obtained by sequentially scanning the external cavity length in the range of $0 < L_{ext}/L^*_{cry} < 1$ display a temporal wave carpet, manifesting different orders of fractional revivals similar to the spatial Talbot revivals [29–32]. In brief, the present result not only confirms a practical way for generating ultrahigh-repetition-rate femtosecond lasers but also reveals an interesting phenomenon of temporally fractional revivals.

2. Principle analysis

As shown in Fig. 1, the present design consists of a monolithic crystal to generate the self-mode-locked pulse train and a partial reflective mirror to form the external FP cavity for repetition-rate multiplication. The frequency spectrum of the monolithic self-mode-locked laser can be expressed as [33]

$$I_{SML}(f) = \sum_{n=-N}^{N} a_n \ \delta(f - f_c - n\, f_{ML}). \qquad (1)$$

where a_n is the weighting coefficient, f_c is the central frequency, $f_{ML} = c/(2L^*_{cry})$ is the longitudinal mode spacing, c is the speed of light in vacuum, $L^*_{cry} = n_r L_{cry}$, n_r is the refractive index of the gain medium, and L_{cry} is the geometric length of the gain medium. The spectral transmission function of the external FP filter with the length of L_{ext} can be derived as [21]

$$T_{FP}(f) = \frac{(1 - R_{oc})(1 - R_{ext})}{(1 - \sqrt{R_{oc}}R^2_{ext} + 4\sqrt{R_{oc}}R_{ext}/c)}, \qquad (2)$$

where R_{oc} is the reflectivity of the output surface of the laser crystal and R_{ext} is the reflectivity of the external FP mirror.

By direct multiplication of Eqs. (1) and (2), we can obtain the frequency spectrum for the self-mode-locked pulses passing through the external FP cavity. To manifest the output spectrum in a realistic way, the Lorentzian function is used to express the δ-function in Eq. (1). The resultant frequency spectrum is then given by

$$I(f) = \frac{1}{\pi}\sum_{n=-N}^{N}\left\{\frac{a_n\,\Gamma_c\ {f_{ML}}^2}{[(f - f_c) - n\ f_{ML}]^2 + (\Gamma_c\ f_{ML})^2} \times \frac{(1 - R_{oc})(1 - R_{ext})}{\left(1 - \sqrt{R_{oc}R_{ext}}\right)^2 + 4\sqrt{R_{oc}R_{ext}}\sin^2\left(\pi\, n\, L_{ext}/L^*_{cry}\right)}\right\}, \qquad (3)$$

where Γ_c is the effective linewidth of the cavity mode. Figure 2 depicts numerical results for the frequency spectrum as a function of the ratio L_{ext}/L^*_{cry} in the range of 0.0−1.0. The values for the parameters are $a_n = 1$, $\Gamma_c = 0.001$, $R_{oc} = 0.98$, $R_{ext} = 0.82$, and $N = 15$. It can be seen that when the external FP cavity length leads to a ratio L_{ext}/L^*_{cry} close to a simple fraction q/p, the frequency spectrum can form a structure with an effective mode spacing to be $p \times f_{ML}$. In other words, the pulse trains with the pth harmonics of the self-mode-locked repetition rate can be effectively obtained by controlling the external FP cavity length to satisfy $L_{ext}/L^*_{cry} = q/p$.

The temporal form for the laser output emitted from the monolithic crystal laser with external FP cavity can be expressed with the Fourier transform of the product of two functions in Eqs. (1) and (2):

$$\Psi(t, L_{ext}) = e^{-i2\pi\, f_c\, t}\sum_{n=-N}^{N} \times \frac{a_n(1 - R_{oc})(1 - R_{ext})\ \exp\left(-i\frac{2\pi\, n}{T}t\right)}{\left(1 - \sqrt{R_{oc}R_{ext}}\right)^2 + 4\sqrt{R_{oc}R_{ext}}\sin^2\left(\pi\, n\, \frac{L_{ext}}{L^*_{cry}}\right)}, \qquad (4)$$

where $T = 1/f_{ML}$ is the fundamental period of the original mode-locked pulses. Figure 3 depicts calculated results

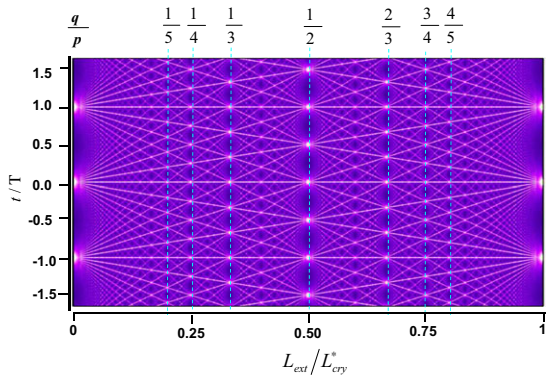

Figure 3 Calculated results for the wave pattern $|\Psi(t, L_{ext})|$ in Eq. (4) with $a_n = 1$, $R_{oc} = 0.98$, $R_{ext} = 0.82$, and $N = 35$.

for the wave pattern $|\Psi(t, L_{ext})|$ in Eq. (4) with $a_n = 1$, $R_{oc} = 0.98$, $R_{ext} = 0.82$, and $N = 35$, where the horizontal and vertical axes are the variables of L_{ext}/L^*_{cry} and t/T, respectively. It can be seen that the periodic pulse trains with pth orders conspicuously occur at the conditions of the external FP cavity length satisfying $L_{ext}/L^*_{cry} = q/p$. Intriguingly, this temporal wave carpet is quite similar to the spatial Talbot revivals, manifesting different orders of fractional revivals [29, 30]. Figures 4(a)–4(h) show numerical results for several temporal structures of the wave patterns $|\Psi(t, L_{ext})|^2$ for the FP cavity length L_{ext} to be a commensurate ratio of the crystal length L^*_{cry} with q/p of 1/5, 1/4, 1/3, 1/2, 2/3, 3/4, 4/5, and 5/6, respectively. The pulse trains clearly reveal the features of pth order harmonics at the conditions of $L_{ext}/L^*_{cry} = q/p$. The analysis indicates the feasibility of generating ultrahigh-repetition-rate lasers from a monolithic mode-locked laser with an external FP cavity.

3. Experimental results and discussion

To perform the experimental exploration, a specially coated Yb:KGW crystal was designed to achieve the self-mode-locked operation [14]. The gain medium was a 5 at.% doped Yb:KGW crystal with a length of 3.05 mm and cut along the n_g-axis. Note that the crystal length was chosen in the

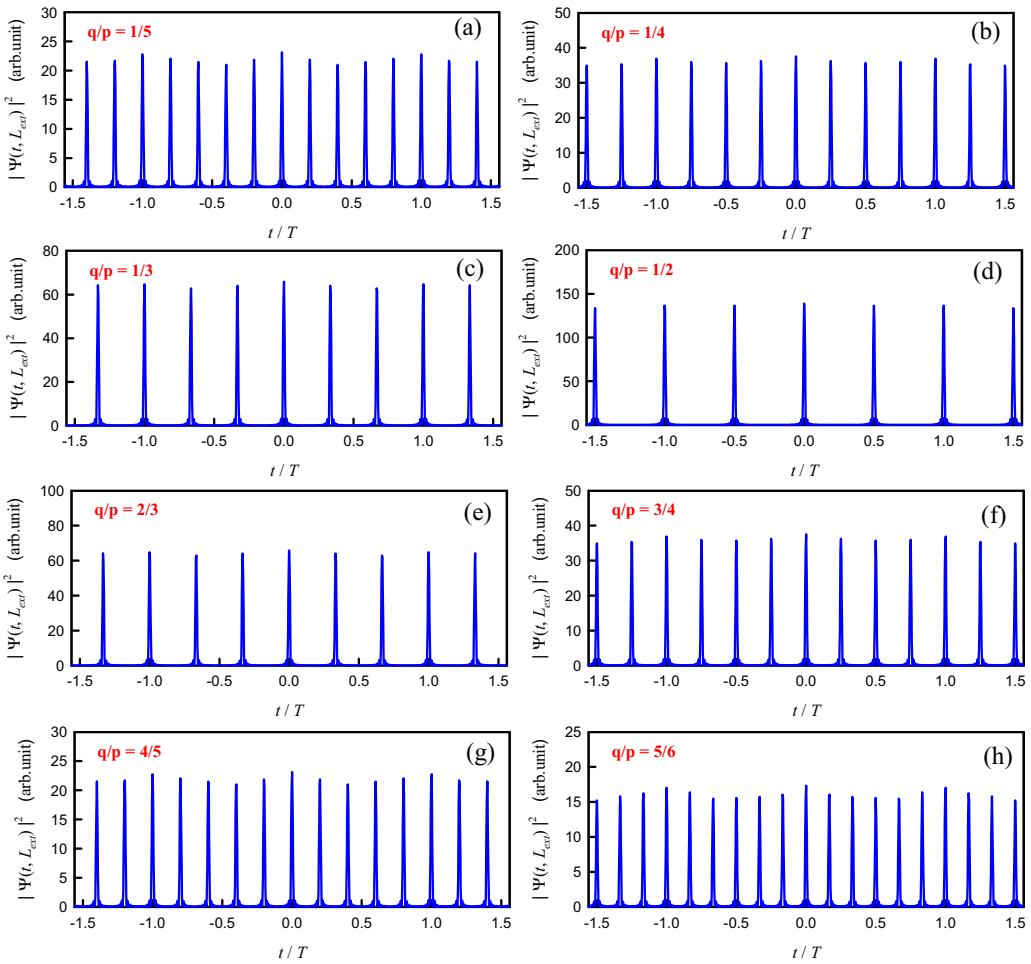

Figure 4 Numerical results for several temporal structures of the wave patterns $|\Psi(t, L_{ext})|^2$ for the FP cavity length at the conditions of $L_{ext}/L^*_{cry} = q/p$: (a) 1/5, (b) 1/4, (c) 1/3, (d) 1/2, (e) 2/3, (f) 3/4, (g) 4/5, and (h) 5/6.

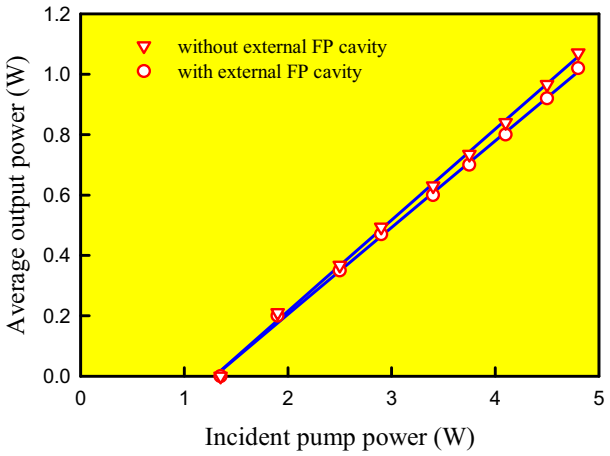

Figure 5 Average output power versus incident pump power for the laser scheme without and with the external FP cavity.

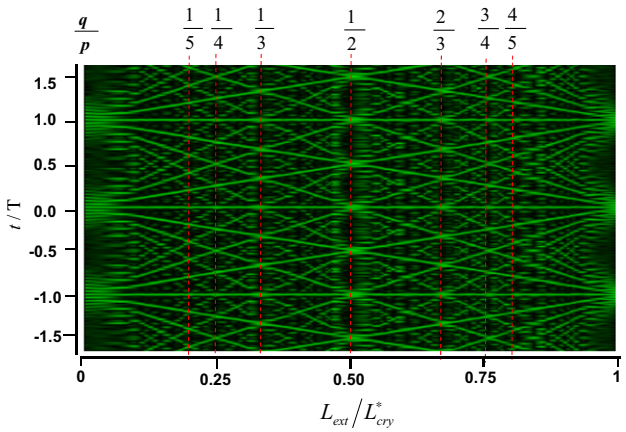

Figure 6 Experimental contour plot formed by all first-order temporal autocorrelation traces obtained by scanning L_{ext} from nearly zero to L^*_{cry}.

range of 3.0 mm to avoid significant re-absorption losses. On Fig. 1, the laser crystal surfaces can be denoted by S1 (the surface that faces the pump source and that acts as the resonator high-reflectivity mirror) and S2 (the opposite side). Side S1 of the crystal was coated for high reflection (R>99.8%) in the range of 1030 nm and 1070 nm and high-transmission (T>95%) at 980 nm to serve as the front mirror. The opposite side S2 was coated for high reflection (R>99%) at 980 nm to increase the absorption efficiency of the pump power and was coated for partial reflection (R≈98%) in the range of 1040 nm and 1060 nm to form the output coupler of the monolithic self-mode-locked operation. The Yb:KGW crystal was wrapped with indium foil and mounted within a water-cooled copper heat sink at 8°C. The pumping source was a 5-W 980-nm fiber-coupled laser diode with a core diameter of 100 μm and a numerical aperture of 0.2. A lens with a focal length of 25 mm was used to focus the pump beam into the laser crystal. The pump spot radius was approximately 110 μm. A flat wedged mirror with 82% reflection at 1050 nm was closely behind the monolithic laser to constitute an external FP cavity.

Figure 5 shows the average output power versus incident pump power for the laser scheme. Without the external FP cavity, it can be seen that the pump threshold is approximately 1.35 W and the average output power is up to 1.07 W at an incident pump power of 4.8 W. Since the average output power is nearly the same for the ratio L_{ext}/L^*_{cry} in the range of 0.0−1.0, the experimental result with $L_{ext}/L^*_{cry} = 0.5$ is only shown for convenience. Clearly, the output power with the external FP cavity only decreases 3–5%, comparing to the result without the feedback cavity.

Since the pulse repetition rate was considerably beyond the measurement range of the contemporary oscilloscope, we employed the methods of first- and second-order autocorrelations to acquire the temporal behavior of the laser output. The first-order autocorrelation trace was attained with a Michelson interferometer (Advantest Q8347) with resolution of 0.003nm that is also able to perform optical spectral analysis by Fourier transforming the first-order field autocorrelation. The second-order autocorrelation trace was obtained with a commercial autocorrelator (APE pulse check, Angewandte Physik & Elektronik GmbH).

Without the external FP cavity, the output of the monolithic laser was found to be in the self-mode-locked operation with the repetition rate of 24 GHz which exactly corresponds to the free spectral range of the optical crystal length. With the external FP cavity, we systematically recorded the traces of the first- and second-order autocorrelations by scanning L_{ext} from nearly zero to L^*_{cry}. It was generally found that the pulse separation and the temporal structure were the same as for the results obtained with the first- and second-order autocorrelation traces. The great resemblance between the first- and second-order autocorrelation traces indicates the phase of the optical spectrum to be nearly constant [33]. Figure 6 shows the experimental contour plot formed by all first-order temporal autocorrelation traces obtained by scanning L_{ext} from nearly zero to L^*_{cry}, where the horizontal and vertical axes are the variables of L_{ext}/L^*_{cry} and t/T, respectively. The overall temporal behavior displays a revival carpet that agrees very well with the numerical patterns shown in Fig. 3. The excellent agreement between the experimental and numerical data not only validates the theoretical analysis but also confirms the laser operation.

Then we further demonstrated the detailed structure of the pulse train in the harmonic operation for the FP cavity length L_{ext} near a commensurate ratio of the crystal length L^*_{cry}. Figures 7(a)−7(j) show the experimental results of the first-order autocorrelation obtained at the average output power of 0.6 W for various harmonic operations with the external cavity lengths L_{ext} of 0.877, 1.023, 1.227, 1.534, 2.046, 3.068, 4.091, 4.602, 4.909, and 5.114 mm, respectively. We clearly find that the characteristics of temporal traces obtained in the commensurate condition of $L_{ext}/L^*_{cry} = q/p$ are equivalent to the so-called harmonically mode-locked oscillations with the pth order

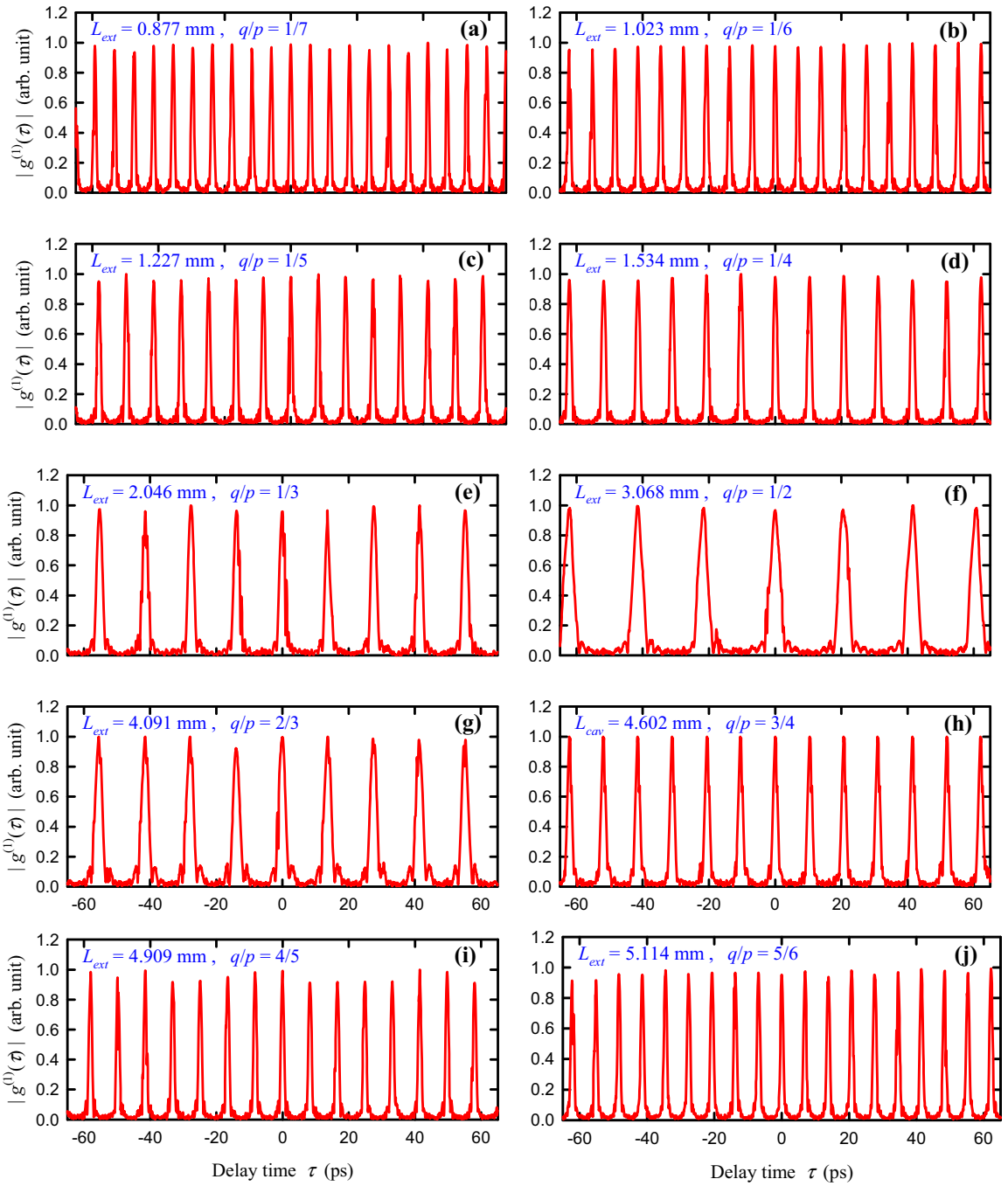

Figure 7 Experimental results of the first-order autocorrelation obtained at the average output power of 0.6 W for various harmonic operations to display the detailed feature of the pulse train with the external cavity lengths L_{ext} of (a) 0.877 mm, (b) 1.023 mm, (c) 1.227 mm, (d) 1.534 mm, (e) 2.046 mm, (f) 3.068 mm, (g) 4.091 mm, (h) 4.602 mm, (i) 4.909 mm, and (j) 5.114 mm.

harmonics of the mode spacing of the monolithic cavity. It is worth noting that the pulse durations for the second ($p = 2$) and third ($p = 3$) harmonics are somewhat wider than the results for higher harmonics due to the difference of lasing spectral widths between lower and higher harmonics. The variation of the spectral width on the harmonic order was not taken into account in the numerical analysis shown in Fig. 4.

Figure 8(a) shows the experimental result for the optical frequency spectrum obtained at the condition of $q/p = 8/9$. The optical spectrum can be seen to center at 284.2 THz with the mode spacing of 216 GHz and the full width at half maximum (FWHM) of 1.08 THz. The FWHM width of the single pulse of the second-order autocorrelation trace is shown in Fig. 8(b). Assuming the sech^2-shaped temporal profile, the pulse duration is estimated to be 330 fs.

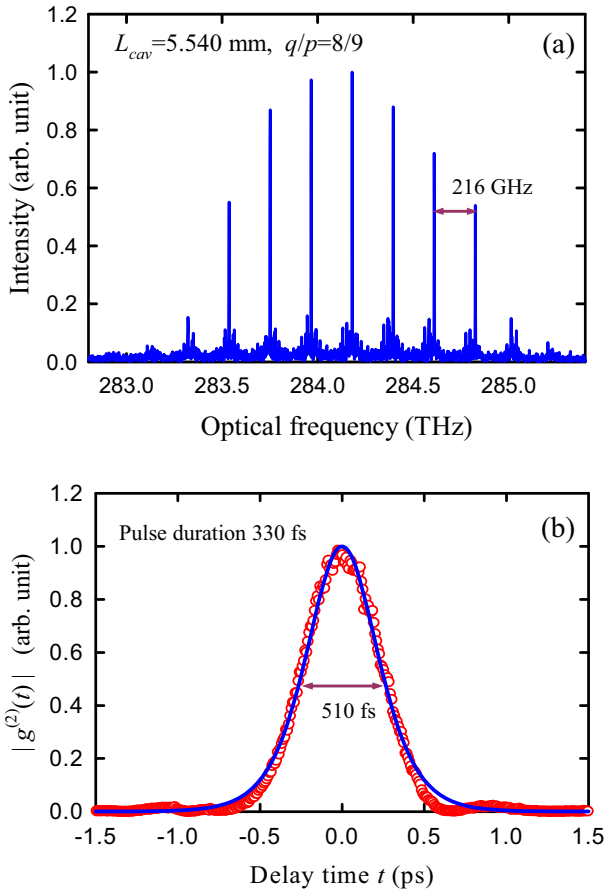

Figure 8 (a) Experimental result for the optical frequency spectrum obtained with the cavity length at the condition of $q/p = 8/9$. (b) FWHM width of a single pulse of the second-order autocorrelation.

Consequently, the time-bandwidth product of the mode-locked pulse is found to be 0.356 that is slightly larger than the Fourier-limited value of 0.315. The chirped pulses mainly come from the group velocity dispersion introduced by the gain medium.

4. Conclusions

In summary, we have developed a novel method to generate sub-terahertz pulse sources by combining a monolithic self-mode-locked laser with a compact scheme of repetition-rate multiplication. With a coated Yb:KGW crystal, we primarily achieved a self-mode-locked operation at a repetition rate of 24 GHz with an average output power exceeding 1.0 W at a pump power of 4.8 W. We then constituted an external Fabry-Perot cavity by employing a partially reflective mirror and the output surface of the laser crystal. We have theoretically and experimentally confirmed that various order harmonics of the mode spacing of the monolithic cavity can be systematically obtained by adjusting the external cavity length to satisfy the commensurate condition. The average output power of the laser output was found to be generally greater than 1.0 W at a pump power of 4.8 W and the maximum pulse repetition rate was up to 216 GHz. With sequentially scanning the external cavity length, it has been intriguingly observed that the overall characteristics of the first-order autocorrelation traces display a similar phenomenon of fractional Talbot revivals in temporal domain. It is believed that the present result can provide more interesting perspectives in the fractional revivals, not only in generating ultrahigh-repetition-rate femtosecond lasers.

Acknowledgment. This work is supported by the National Science Council of Taiwan (Contract No. MOST -10 3 -2 112 -M-009-0 16 -MY3).

Received: 5 June 2014, **Revised:** 19 September 2014, **Accepted:** 25 September 2014

Published online: 22 October 2014

Key words: sub-terahertz repetition rates, mode-locked laser, Fabry-Perot feedback, monolithic cavity.

References

[1] V. Gerginov, C. E. Tanner, S. A. Diddams, A. Bartels, and L. Hollberg, Opt. Lett. **30**, 1734–1736 (2005).
[2] H. Hu, H. C. H. Mulvad, C. Peucheret, M. Galili, A. Clausen, P. Jeppesen, and L. K. Oxenløwe, Opt. Express **19**, 343–349 (2011).
[3] M. Pelton, J. E. Sader, J. Burgin, M. Liu, P. Guyot-Sionnest, and D. Gosztola, Nat. Nanotechnol. **4**, 492–495 (2009).
[4] S. T. Cundiff and A. M. Weiner, Nat. Photonics **4**, 760–766 (2010).
[5] H. A. Haus, J. Sel. Top. Quantum Electron. **6**, 1173–1185 (2000).
[6] S. Pekarek, T. Südmeyer, S. Lecomte, S. Kundermann, J. M. Dudley, and U. Keller, Opt. Express **19**, 16491–16497 (2011).
[7] P. Klopp, U. Griebner, M. Zorn, and M. Weyers, Appl. Phys. Lett. **98**, 071103 (2011).
[8] M. Hoffmann, O. D. Sieber, V. J. Wittwer, I. L. Krestnikov, D. A. Livshits, Y. Barbarin, T. Südmeyer, and U. Keller, Opt. Express **19**, 8108–8116 (2011).
[9] T. J. Kippenberg, R. Holzwarth, and S. A. Diddams, Science **339**, 555–559 (2011).
[10] T. Herr, K. Hartinger, J. Riemensberger, C. Y. Wang, E. Gavartin, R. Holzwarth, M. L. Gorodetsky, and T. J. Kippenberg, Nature Photon. **6**, 480–487 (2012).
[11] J. S. Levy, A. Gondarenko, M. A. Foster, A. C. Turner-Foster, A. L. Gaeta, and M. Lipson, Nature Photon. **4**, 37–40 (2010).
[12] A. B. Matsko, A. A. Savchenkov, W. Liang, V. S. Ilchenko, D. Seidel, and L. Maleki, Opt. Lett. **36**, 2845–2847 (2011).
[13] H. Liu, J. Nees, and G. Mourou, Opt. Lett. **26**, 1723–1725 (2001).
[14] W. Z. Zhuang, M. T. Chang, H. C. Liang, and Y. F. Chen, Opt. Lett. **38**, 2596–2599 (2013).
[15] A. A. Lagatsky, A. R. Sarmani, C. T. A. Brown, W. Sibbett, V. E. Kisel, A. G. Selivanov, I. A. Denisov, A. E. Troshin, K. V. Yumashev, N. V. Kuleshov, V. N. Matrosov, T. A.

Matrosova, and M. I. Kupchenko, Opt. Lett. **30**, 3234–3236 (2005).
[16] G. Q. Xie, D. Y. Tang, L. M. Zhao, L. J. Qian, and K. Ueda, Opt. Lett. **32**, 2741–2743 (2007).
[17] S. Uemura and K. Torizuka, Appl. Phys. Express **1**, 012007 (2008).
[18] H. C. Liang, R. C. C. Chen, Y. J. Huang, K. W. Su, and Y. F. Chen, Opt. Express **16**, 21149–21154 (2008).
[19] H. C. Liang, Y. J. Huang, W. C. Huang, K. W. Su, and Y. F. Chen, Opt. Lett. **35**, 4–6 (2010).
[20] H. C. Liang, Y. J. Huang, Y. C. Lin, T. H. Lu, Y. F. Chen, and K. F. Huang, Opt. Lett. **34**, 3842–3844 (2009).
[21] K. Yiannopoulos, K. Vyrsokinos, E. Kehayas, N. Pleros, K. Vlachos, H. Avramopoulos, and G. Guekos, IEEE Photon. Technol. Lett. **15**, 1294–1296 (2003).
[22] P. Petropoulos, M. Ibsen, M. N. Zervas, and D. J. Richardson, Opt. Lett. **25**, 521–523 (2000).
[23] B. Xia and L. R. Chen, IEEE Photon. Technol. Lett. **18**, 1999–2001 (2006).
[24] C. B. Huang, Z. Jiang, D. Leaird, J. Caraquitena, and A. Weiner, Laser Photonics Rev. **2**, 227–248 (2008)
[25] M. A. Preciado and M. A. Muriel, Opt. Lett. **33**, 962–964 (2008).
[26] R. Slavík and S. LaRochelle, Optics Communications **247**, 307–312 (2005).
[27] J. Azaña and M. A. Muriel, Appl. Opt. **38**, 6700–6704 (1999).
[28] S. Longhi, M. Marano, P. Laporta, and V. Pruneri, IEEE Photon. Technol. Lett. **12**, 1498–1500 (2000).
[29] M. V. Berry and S. Klein, J. Mod. Opt. **43**, 2139–2164 (1996).
[30] W. B. Case, M. Tomandl, S. Deachapunya, and M. Arndt, Opt. Express **17**, 20966–20974 (2009).
[31] M. V. Berry, I. Marzoli, and W. P. Schleich, Phys. World **14**, 39–44 (2001).
[32] M. J. Mark, E. Haller, J. G. Danzl, K. Lauber, M. Gustavsson, and H.-C. Näger, New J. Phys. **13**, 085008 (2011).
[33] A. M. Weiner, Ultrafast Optics (John Wiley & Sons Inc., Hoboken, NJ, 2009).